Stability of Single Axis Gyros in a Circular Orbit

WILLIAM T. THOMSON*
University of California, Los Angeles, Calif.

The stability of single axis gyros mounted on a vehicle in circular motion about a central force field is examined for several orientations of the spin vector and output axis. When the orientation of the output axis is in the radial or tangential direction of the orbit, as in the case of pitch or roll sensors, the stability is dependent on the ratio of the spin angular velocity to the vehicle angular velocity around the orbit and the ratio of the moments of inertia of the gyro wheel. When the orientation of the output axis is fixed in inertial space, as in an inertial platform, the equations of motion are of the Mathieu type. The stability in this case is independent of the spin angular velocity of the gyro wheel and is a function of the moment of inertia ratio of the wheel, the angular velocity of the vehicle around the orbit, and the desired orentation of the spin velocity vector.

Introduction

WHEN the spin axis of a gyro is maintained in a direction normal to the plane of motion of the vehicle, there can be no change in the spin angular momentum vector due to the motion of the vehicle in the orbit plane. If, however, the spin axis deviates from this normal position in any direction, the component of the spin angular momentum vector in the orbit plane is subject to change in direction, depending on the motion of the vehicle. Evans[1] has shown that even in a torque-free environment the single axis gyro becomes unstable for all values of the moment of inertia ratio C/A when the spin angular velocity ω_s is directed in the opposite sense to the orbit angular velocity ω_0. When the differential gravity torque is considered, this result is altered so that stability depends on both ω_s/ω_0 and C/A. In the case where the output axis is radial or tangential to the orbit axes, the stability criterion can be deduced as a special case of the two-axis motion discussed previously by Thomson[2] and Kane.[3] The various cases will be discussed in terms of the orientation of the spin vector and the output axis.

Case 1: Roll Gyro

In this case the spin vector is normal to the orbit plane with the output axis tangent to the orbit path. Figure 1 shows the gyro orientation and the coordinate system that is identical to that of Ref. 2. With $\theta_3 = 0$,† the first of Eqs. (5) of Ref. 2 reduces to

$$I_1\ddot{\theta}_1 - \omega_0^2\theta_1(I_1 - I_2) + I_2\omega_s\omega_0\theta_1 = 3\omega_0^2(I_1 - I_2)\theta_1 \quad (1)$$

where the term on the right side is due to the differential gravity torque. Letting the moment of inertia about the spin axis be $I_2 = C$ and that about the transverse axis be $I_1 = I_3 = A$, the equation can be rewritten as

$$\ddot{\theta}_1 + \omega_0^2(C/A)[(\omega_s/\omega_0) + 4 - 4(A/C)]\theta_1 = 0 \quad (2)$$

Stability is insured if

$$[(\omega_s/\omega_0) + 4 - 4(A/C)] > 0 \quad (3)$$

which defines the stable and unstable regions as plotted in Fig. 2. Since C/A can never be greater than 2, the practical region for a long pencil-like rotor to a flat disk lies in the region $0 < C/A < 2$.

In general, $\omega_s \gg \omega_0$, and Eq. (2) reduces to

$$\ddot{\theta}_1 + [(C/A)\omega_0\omega_s]\theta_1 = 0 \quad (4)$$

which indicates that spin in the opposite sense to ω_0 results in an unstable gyro for all values of C/A. In Eq. (4), $C\omega_s\theta_1$ is the component of h in the plane of the orbit, and its rate of change $\omega_0(C\omega_s\theta_1)$ can only be supplied by the accelerating torque $A\ddot{\theta}_1$ since axis 1 is moment free.

Of course there will be a torque about the axis 3 since its rotation is restrained, and it can be determined from the second of Eqs. (5), Ref. 2, by letting $\theta_3 = \ddot{\theta}_3 = 0$, i.e., $L_3 = \omega_0\dot{\theta}_1(2I_1 - I_2) - I_2\omega_s\dot{\theta}_1$.

If the output axis is not free but restrained by a restoring spring $-k\theta_1$, Eq. (3) for the stability is replaced by

$$[(\omega_s/\omega_0) + 4 - 4(A/C) + (k/C\omega_0^2)] > 0 \quad (5)$$

which increases the stable region to the dotted curve of Fig. 2.

Although Eq. (4) is applicable to cases where $\omega_s \gg \omega_0$, one should not overlook the fact that instability is possible for large positive values of ω_s/ω_0 with rotors of small C/A.

Case 2: Pitch Gyro

In this case the spin vector is normal to the orbit plane with the output axis in the radial direction of the orbit. For the output axis pointing towards the focus of the central force as shown in Fig. 3, the gravity torque on the gyro wheel is zero. The second of Eqs. (5) in Ref. 2 with $\theta_1 = 0$ then reduces to

$$I_1\ddot{\theta}_3 + \omega_0^2\theta_3(I_2 - I_1) + I_2\omega_s\omega_0\theta_3 = 0 \quad (6)$$

or

$$\ddot{\theta}_3 + \omega_0^2(C/A)[(\omega_s/\omega_0) + 1 - (A/C)]\theta_3 = 0 \quad (7)$$

The system is then stable if

$$[(\omega_s/\omega_0) + 1 - (A/C)] > 0 \quad (8)$$

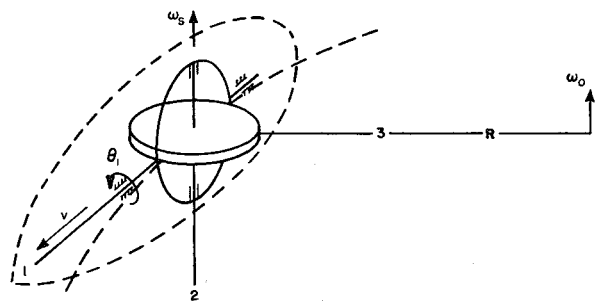

Fig. 1 Gyro output axis tangent to orbit

Received February 14, 1963.

* Professor of Engineering; also Consultant, Space Technology Laboratories, Inc.

† It is assumed that the gyro is mounted on a platform that allows no pitch motion θ_3 of the output axis.

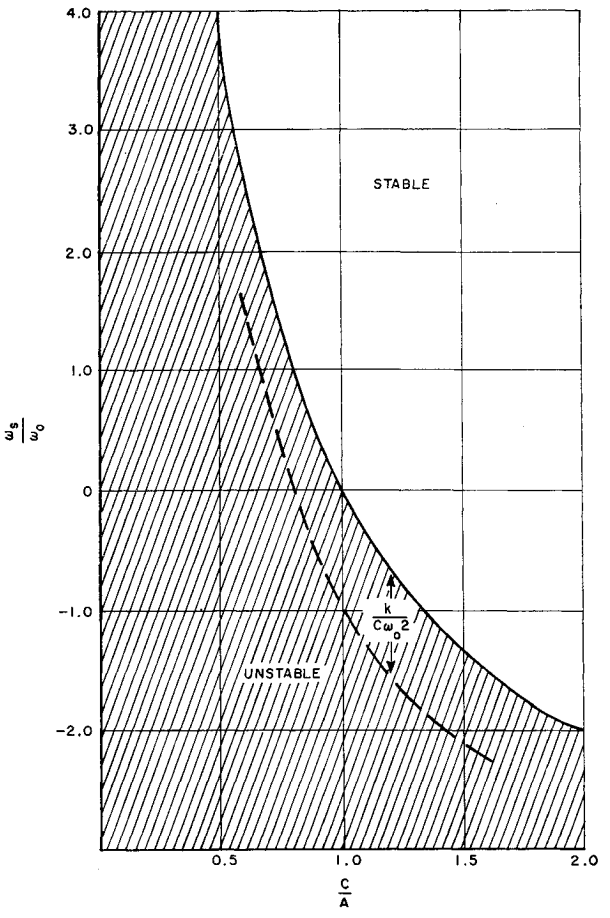

Fig. 2 Stable and unstable regions for gyro of Fig. 1

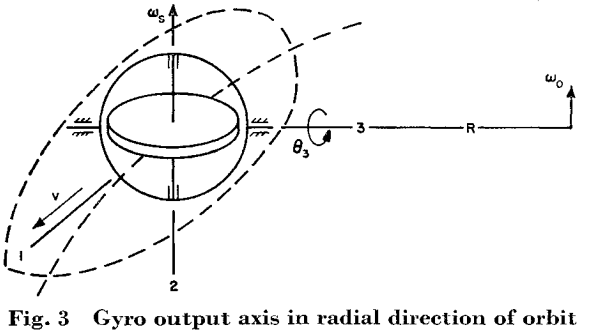

Fig. 3 Gyro output axis in radial direction of orbit

and the stable and unstable regions are shown in Fig. 4.

Here again for $\omega_s \gg \omega_0$ instability is encountered when ω_s is of opposite sense to ω_0 as in case 1. Also, conclusions for case 1 regarding the restoring spring apply equally well here.

Case 3

In this case the output axis is fixed inertially with the spin vector normal to the orbit plane. With the output axis fixed in direction in the orbit plane as shown in Fig. 5, the components for the torque equation

$$L = \dot{h} + \omega \times h \tag{9}$$

are

$$\omega_1 = \omega_2 = 0 \qquad h_1 = 0$$
$$\omega_3 = \dot{\theta}_3 \qquad h_2 = -C\omega_s$$
$$h_3 = A\dot{\theta}_3$$

The gravity torque L about the gyro axes 1, 2, and 3 now is also a function of the orbit angle $\Phi = \omega_0 t$ as derived in the

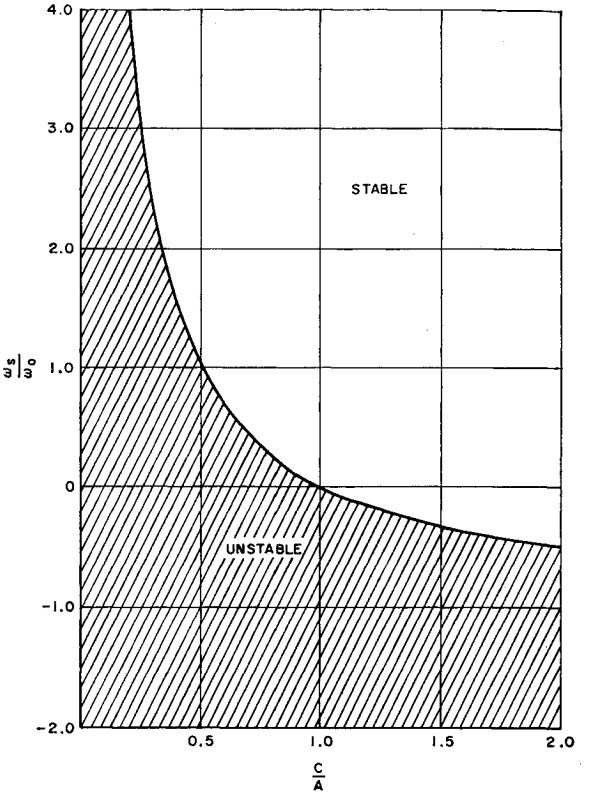

Fig. 4 Stable and unstable regions for the gyro of Fig. 3

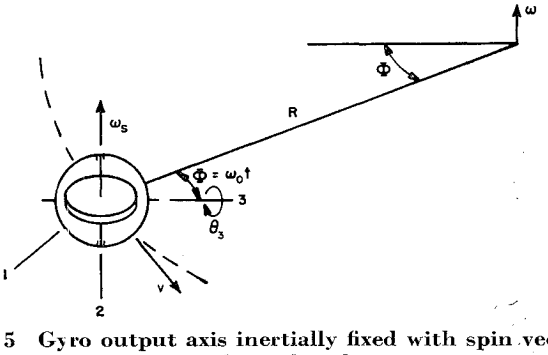

Fig. 5 Gyro output axis inertially fixed with spin vector normal to orbit plane

Appendix. Since $\theta_1 = \theta_2 = 0$ and θ_3 is restricted to small values, Eq. (A6) is used:

$$L_3 = \tfrac{3}{2}\omega_0^2(A - C)\theta_3(1 - \cos 2\omega_0 t) \tag{10}$$

The torque equation about the axis 3 is then

$$\ddot{\theta}_3 + (3\omega_0^2/2)[(C/A) - 1](1 - \cos 2\omega_0 t)\theta_3 = 0 \tag{11}$$

which may be put into the standard form of the Mathieu equation[4]:

$$(d^2y/dz^2) + (a - 2q\cos 2z)y = 0 \tag{12}$$

by letting $\omega_0 t = z$. Equation (11) then becomes

$$(d^2\theta_3/dz^2) + \tfrac{3}{2}[(C/A) - 1](1 - \cos 2z)\theta_3 = 0 \tag{13}$$

so that

$$a = 2q = \tfrac{3}{2}[(C/A) - 1] \tag{14}$$

Figure 6 shows the stable and unstable regions of Eq. (12) and the straight line indicated by Eq. (14). One thus finds along the line $a = 2q$ alternately stable and unstable values of $a = \frac{3}{2}[(C/A) - 1]$. However, since C/A lies between 0 and 2, a for the gyro is restricted between $\pm\frac{3}{2}$ which enables one to define the stable and unstable regions as shown

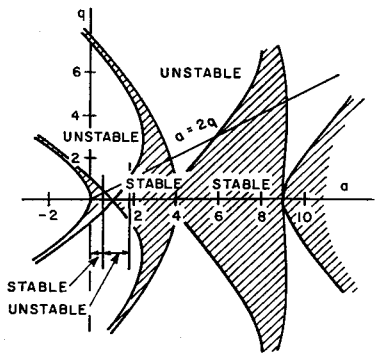

Fig. 6 Stable and unstable regions for the Mathieu equation

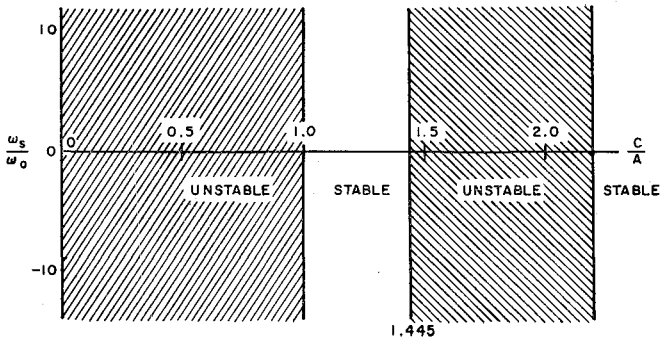

Fig. 7 Stable and unstable regions for the gyro of Fig. 5

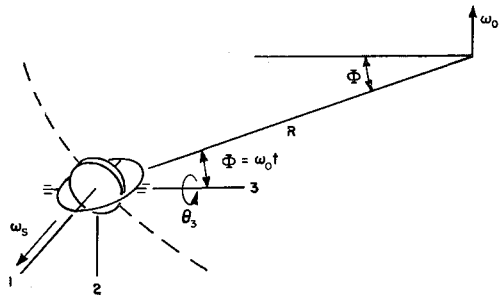

Fig. 8 Gyro output axis inertially fixed with spin vector in the orbit plane

in Fig. 7, i.e., the first stable region on the line $a = 2q$ lies between $a = 0$ and $a = 0.666$. Therefore,

$$0 < \tfrac{3}{2}[(C/A) - 1] < 0.666$$

or

$$1.0 < (C/A) < 1.445$$

It should be noted that the magnitude of the spin angular velocity ω_s does not enter into this case.

Case 4

This is the same as case 3 with the spin axis along axis 1 in the orbit plane, as shown in Fig. 8. The equation of motion for this case is identical to that of case 3 except for the sign before ω_0^2 which is negative:

$$\ddot{\theta}_3 - (3\omega_0^2/2)[(C/A) - 1](1 - \cos 2\omega_0 t)\theta_3 = 0$$

Thus the system is stable only if

$$0 < -\tfrac{3}{2}[(C/A) - 1] < 0.666$$

or

$$\tfrac{5}{9} < (C/A) < 1.0$$

as shown in Fig. 9.

It is also possible to orient the output axis inertially along axis 1 with the spin vector normal and parallel to the orbit plane. However, these orientations are equivalent to moving the reference for the measurement of Φ by 90°, and no new stability results are obtained.

Appendix

The equation for the differential gravity torque about axes 1, 2, 3 referenced to rotating orbit axes O_1, O_2, O_3, where O_1 is tangent to the orbit path, O_2 is normal to the orbit plane, and O_3 is radial toward the central force focal point, was derived in the Appendix of Ref. 2. Now this is extended to the case where the reference axes O_1, O_2, O_3 remain fixed in inertial space with O_2 normal to the orbit plane and O_3 parallel to a fixed radial reference. The radial vector to the moving vehicle then makes an angle $\Phi = \omega_0 t$ with the O_3 axis as shown in Fig. 10.

With $\rho = xi + yj + zk$ defining the mass element dm with i, j, k as unit vectors along the body axes 1, 2, 3, the torque equation is

$$\mathbf{L} = \frac{3K}{R^3}\int \frac{(\mathbf{R}\cdot\boldsymbol{\rho})(\boldsymbol{\rho}\times\mathbf{R})dm}{R^2} \qquad \text{(A1)}$$

where $\mathbf{R}$ is the orbital radius vector to the vehicle center of mass. The equation differs from that of Ref. 2 only in $\mathbf{R}$, which now is a function of Φ as well as $\theta_1,\theta_2,\theta_3$, and is equal to

$$\mathbf{R} = R_0[\cos\Phi(i\alpha_1 + j\beta_1 + k\gamma_1) + \sin\Phi(i\alpha_2 + j\beta_2 + k\gamma_2)] \qquad \text{(A2)}$$

where

$$\begin{aligned}
\alpha_1 &= \sin\theta_2 \\
\beta_1 &= -\cos\theta_2 \sin\theta_1 \\
\gamma_1 &= -\cos\theta_2 \cos\theta_1 \\
\alpha_2 &= \cos\theta_2 \cos\theta_3 \\
\beta_2 &= -\cos\theta_1 \sin\theta_3 + \sin\theta_1 \sin\theta_2 \cos\theta_3 \\
\gamma_2 &= \cos\theta_1 \sin\theta_2 \cos\theta_3 + \sin\theta_1 \sin\theta_3
\end{aligned} \qquad \text{(A3)}$$

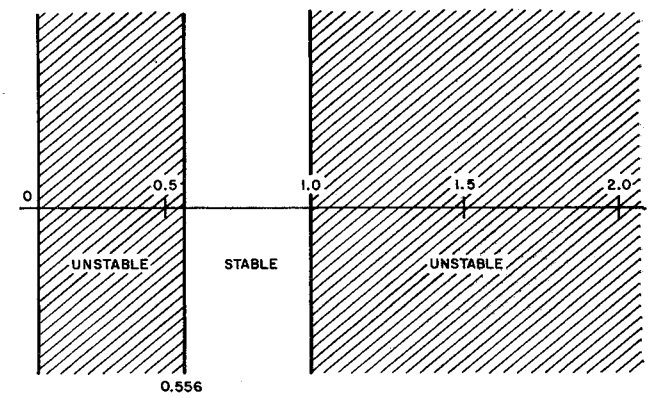

Fig. 9 Stable and unstable regions for the gyro of Fig. 8

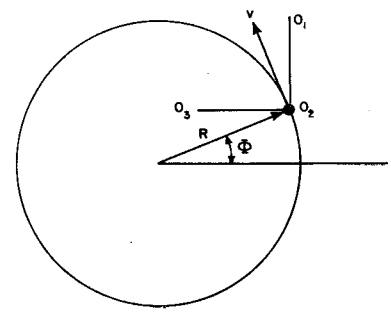

Fig. 10 Gravity torque for inertial axes O_1, O_2, O_3

The torque equation then becomes

$$\mathbf{L}(R^3/3K) = i(I_3 - I_2)[\beta_1\gamma_1 \cos^2\Phi + \beta_2\gamma_2 \sin^2\Phi + (\beta_1\gamma_2 + \beta_2\gamma_1) \cos\Phi \sin\Phi] + j(I_1 - I_3) \times [\alpha_1\gamma_1 \cos^2\Phi + \alpha_2\gamma_2 \sin^2\Phi + (\alpha_2\gamma_1 + \alpha_1\gamma_2) \cos\Phi \sin\Phi] + k(I_2 - I_1)[\alpha_1\beta_1 \cos^2\Phi + \alpha_2\beta_2 \sin^2\Phi + (\alpha_1\beta_2 + \alpha_2\beta_1) \cos\Phi \sin\Phi] \quad (A4)$$

When the angles θ_1, θ_2, θ_3 are small deviations from the reference axes, the torque reduces to the following components:

$$L_1 = 3\omega_0^2(I_3 - I_2)(\theta_1 \cos^2\Phi + \theta_3 \sin\Phi \cos\Phi)$$

$$L_2 = 3\omega_0^2(I_3 - I_1)(\theta_2 \cos^2\Phi - \theta_2 \sin^2\Phi + \sin\Phi \cos\Phi) \quad (A5)$$

$$L_3 = 3\omega_0^2(I_1 - I_2)(\theta_3 \sin^2\Phi + \theta_1 \sin\Phi \cos\Phi)$$

For the symmetric gyro of case 3, $I_1 = I_3 = A$ and $I_2 = C$, and the torque about axis 3 reduces to

$$L_3 = \tfrac{3}{2}\omega_0^2(A - C)\theta_3(1 - \cos 2\Phi) \quad (A6)$$

References

[1] Evans, H. W., "Analysis of one and two-gimbal attitude gyros in a satellite application," Rept. SM-39040, Douglas Aircraft Co., Inc., Santa Monica, Calif. (October 25, 1961).

[2] Thomson, W. T., "Spin stabilization of attitude against gravity torque," J. Astronaut. Sci. **IX**, 31–33 (Spring 1962).

[3] Kane, T. R., Discussion and correction of stability curve presented in Ref. 2, J. Astronaut. Sci. **IX**, 108–109 (1962).

[4] Cunningham, W. J., *Introduction to Nonlinear Analysis* (McGraw-Hill Book Co. Inc., New York, 1958), pp. 270–274.

JULY 1963 AIAA JOURNAL VOL. 1, NO. 7

Design of Lunar and Interplanetary Ascent Trajectories

VICTOR C. CLARKE JR.*

Jet Propulsion Laboratory, California Institute of Technology, Pasadena, Calif.

The near-Earth or "ascent" portion of lunar and interplanetary trajectories is investigated. Of particular interest is the matching of the powered-flight and coasting phases. To achieve a suitable match, consideration of vehicle-related engineering constraints, payload, and geometrical and energy requirements imposed by the extraterrestrial trajectory is essential. The geometrical constraints and trajectory shaping are treated in detail. To satisfy these constraints, direct-ascent and parking-orbit types of trajectories are investigated and compared. Advantages and disadvantages of each are noted. The superiority of the parking-orbit type is illustrated. It is shown that this type has consistently greater payload capability and provides a convenient method of launch-time delay compensation. Finally, injection locations of Mars and Venus trajectories using parking orbits are mapped.

I. Introduction

THE initial phases of lunar and interplanetary trajectories possess certain common properties that permit a unified analytical treatment of both at the same time. These common properties are primarily geometrical in nature. In this paper, the chief consideration is that phase of flight from launch until the time when the spacecraft is essentially traveling radially outward from the Earth. This phase of flight is termed the "ascent" phase. As will be seen, the design of the ascent trajectory is influenced heavily by several factors.

For purposes of obtaining a gross understanding of ascent trajectory design, it is worthwhile to assume the two-body approximation that the near-Earth path of a lunar trajectory is an ellipse or a hyperbola and the near-Earth path of an interplanetary trajectory is a hyperbola. In actual practice, of course, perturbative effects of Earth's oblateness and celestial bodies, as needed, must be included.

The chief problem of ascent trajectory design is that of matching the powered portions of flight to the final coasting portion. The interaction of these two portions of flight is quite strong. For example, an infinite number of physically realizable ascent trajectories will produce overall lunar or interplanetary flights that satisfy the mission requirement. However, only a small set of these is suitable from a practical standpoint. The practicality of a set of trajectories must be based on engineering considerations such as payload weight, guidance, tracking and telemetry, reliability, vehicle-related constraints, etc. Thus, engineering considerations strongly determine the ascent trajectory in conjunction with the requirements of the overall trajectory.

It is the purpose of this paper to examine the characteristics of lunar and interplanetary ascent trajectories and the factors that determine them. Chief among these factors are the powered-flight phases and the geometrical constraints imposed by the overall trajectory. The geometrical constraints will be considered first.

Received by IAS July 5, 1962; revision received December 28, 1962. This paper presents the results of one phase of research carried out at the Jet Propulsion Laboratory, California Institute of Technology, under Contract NAS7-100, sponsored by NASA.

* Engineering Group Supervisor.

II. Geometrical Properties

Three geometrical properties that strongly influence the ascent trajectory are launch site location, the outward radial direction, and launch azimuth.

A. Launch Location

The first property, launch site location, is an independent variable of the geometry problem which is not changed easily because of the great cost and logistic, communication, and political problems involved. Thus, for firings from the United States, it is logical to assume the launch facility at Cape Canaveral, Atlantic Missile Range (AMR) for our purposes. Lunar and interplanetary launchings from the launch facility of the Pacific Missile Range (PMR) are unde-